Investigation of a Metamaterial Absorber by Using Reflection Theory Model

Cheng Yang[1, *], Han Xiong[2], and Xiao Pan Li[3]

Abstract—Metamaterial absorber (MMA), as a kind of new-style artificial absorption material, has been extensively researched and discussed. Currently, however, the research focuses mainly on the development and application of the novel structure MMA, and only little work is aimed at the physical mechanism of the MMA. In order to deeply understand the absorption mechanism, in this paper, the numerical simulation results of an MMA are given. Then, based on the reflection theory modal, the numerical simulation results are well discussed and explained in detail. It is found that the theoretical results agree well with that of the simulation, which suggests that the reflection theory modal is effective for analyzing the absorption mechanism of the MMA. The main contributions of this paper are to quantitatively discuss and explain the absorption mechanism of the MMA by using the reflection theory and thus offer a consultation in design and fabrication of the advanced MMA for engineers.

1. INTRODUCTION

Metamaterial absorber (MMA) is a new kind of synthetic electromagnetic (EM) absorbing materials that may not be found in nature with special structure, which has excellent EM properties, such as negative refractive index [1, 2], perfect lens [3], and invisible cloak [4]. Since MMA was first put forward by Landy et al. in 2008 [5], it has attracted widespread attention of the science community, due to the broad applications of the MMA in many fields, for example, miniaturization for antennas [6], stealth technology [7], thermal detectors [8, 9], and the miniaturization of microwave device [10]. Over the past few years, most researches on the MMA have been concentrated on the design of MMA showing excellent performance within single-band, multi-band and broad-band [11–15], operations at various frequency spectra scaled from microwave to optical frequencies [16–24], by using different metamaterial resonators. Among these researches, however, few works paid attention to the analysis of the theories for the physic mechanisms, which is necessary for an in-depth study of the MMA.

Meanwhile, some research works have been done in theoretical approaches to explain the physics mechanism of the MMA in recent years. In current literature, several theoretical methods have been presented to reveal the absorption mechanism, which include impedance matching theory [25], equivalent circuit approach [26], transmission line circuit theory [27] and interference theory [28]. Unfortunately, the above mentioned several methods have some limitations and demerits. By using impedance matching theory, the available analysis of absorption mechanism on the MMA is qualitative but not quantitative, so it cannot be applied to numerical analysis. Equivalent circuit approach and transmission line theory fail to explain the physic mechanism for the MMA in oblique incidence condition, which can only be applied to normal incidence condition. Moreover, the interference theory has a few limitations in discussing the relationship between the changing absorptivity and spacer thickness. To date, however,

little attention has been paid to analyzing the effect of the spacer thickness, incident angles, polarization angles, effective dielectric parameters, and absorption frequency on the absorption properties. In fact, it is very important for fully and correctly understanding the absorption mechanism to analyze the effect of the spacer thickness, incident angles, polarization angles, effective dielectric parameters, and absorption frequency on the absorption properties completely. Furthermore, the analytical method on the MMA introduced in our paper will provide consultation to engineers in design and fabrication of the advanced MMA, so that they can fully understand the relationship between the constitutive parameters and the absorption properties.

In this paper, an extended reflection theory model is used with the purpose to completely reveal the absorption mechanism for the MMA. By comparing with numerical simulations, the validity of the theoretical model is verified. It is worth noting that the absorption mechanism of the MMA has not been fully analyzed in the previous studies. However, the method presented in this paper can completely investigate the influences of structure parameters on the absorption properties, including the spacer thickness, incident angles, polarization angles, effective dielectric parameters, and absorption frequency. Most remarkably, our research is more focused on quantitative analysis than the previous studies.

2. EXTENDED REFLECTION THEORY

A schematic diagram of the single-metamaterial absorber employed in this research is shown in Figure 1. It is a typical single-metamaterial absorber structure, composed of an upper metal pattern layer, intermediate medium layer with thickness d and a bottom metal plane. A similar cross-shaped structure has been developed and applied to many analyses of MMAs [29–31], which has certain representativeness, so this structure is used in this paper. The EM wave is radiated to the surface of the MMA slab. In this paper, only the transverse electric (TE) wave incidence case is considered. Here, we set the thickness of the upper metal pattern layer equal to zero. The incident angle and refractive angle are set to θ and α, respectively. It is assumed that the medium layer is homogeneous and isotropic. k_0, ε_0, μ_0, Z_0 and k_1, ε_1, μ_1, Z_1 are the complex wave number, dielectric permittivity, magnetic permeability and intrinsic impedance in the air and the medium layer, respectively. Because of metallicity of the substrate, the substrate's effective impedance is $Z = 0$. According to [32], when the incident waves are TE-polarized wave, the expressions of the effective EM parameters of the medium layer can be written as follows:

If $Z_{\lambda 1 eff} < Z_{0 eff}$

$$
\begin{cases}
\varepsilon_1' = \dfrac{\pi c}{2d\omega} c \tanh\left(\dfrac{\pi}{2}\tan\delta\right) \dfrac{1+\sqrt{1-A(\omega)}}{1-\sqrt{1-A(\omega)}} \dfrac{\cos\theta}{\cos^2\alpha} \\
\mu_1' = \dfrac{\pi c}{2d\omega} \tanh\left(\dfrac{\pi}{2}\tan\delta\right) \dfrac{1-\sqrt{1-A(\omega)}}{1+\sqrt{1-A(\omega)}} \dfrac{1}{\cos\theta}
\end{cases}
\tag{1}
$$

If $Z_{\lambda 1 eff} > Z_{0 eff}$

$$
\begin{cases}
\varepsilon_1' = \dfrac{\pi c}{2d\omega} c \tanh\left(\dfrac{\pi}{2}\tan\delta\right) \dfrac{1-\sqrt{1-A(\omega)}}{1+\sqrt{1-A(\omega)}} \dfrac{\cos\theta}{\cos^2\alpha} \\
\mu_1' = \dfrac{\pi c}{2d\omega} \tanh\left(\dfrac{\pi}{2}\tan\delta\right) \dfrac{1+\sqrt{1-A(\omega)}}{1-\sqrt{1-A(\omega)}} \dfrac{1}{\cos\theta}
\end{cases}
\tag{2}
$$

where ε_1' and μ_1' are the real part of dielectric permittivity and magnetic permeability of the medium layer, respectively. $A(\omega)$ is the absorptivity of MMA, $Z_{\lambda 1 eff}$ the input impedance, and $Z_{0 eff} = \sqrt{\mu_0/\varepsilon_0}\big/\cos\theta$ the effective impedance for TE-polarized wave in the air.

The above expressions shows the relationships among the real part of dielectric permittivity or permeability, angle of incidence, angle of refraction, frequency, thickness of the medium layer, loss tangent, and absorptivity. Here, the relationship between the angle of incidence θ and angle of refraction α stems from the Snell's law. In fact, it is simpler and intuitive to analyze the relationship between the absorption properties and structure parameter through the above expressions. In the next section, to confirm that the universal validity of the above expressions is effective, the numerical simulations of
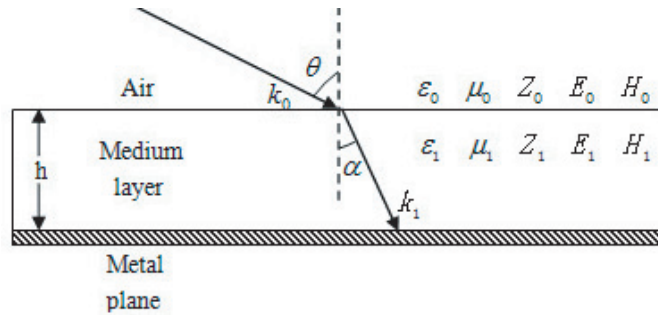
Figure 1. Structure schematic of a single-layer absorber.

a MMA will be shown. Furthermore, based on the above expressions, the MMA will be analyzed and discussed.

3. STRUCTURE DESIGN AND SIMULATIONS

The schematic view of the unit cell of the analyzed cruciform structure absorber is depicted in Figure 2. The unit cell is made up of three layers, including upper metal pattern layer, intermediate medium layer and bottom metal plane. The three layers are formed with copper, FR4, and copper from top to bottom, respectively. The electrical conductivity of the copper with thickness of 0.017 mm is 5.8×10^7 S/m. The relative permittivity of the FR4 substrate with thickness of 0.5 mm is $4.4(1 - j0.04)$. The other size parameters of the unit cell are $L = 10$ mm, $l = 7$ mm, $w = 1$ mm, $e = 2.6$ mm, $b = 0.4$ mm, which are obtained by applying the classical simulation software HFSS based on the finite element method. Figure 3 shows the simulated absorptivity of the absorber. It can be seen that there is an absorptivity peak at 11.5 GHz with absorption of 99.99%.

Firstly, the influence of the dielectric layer thickness d on the absorption properties of the MMA is investigated under the normal incidence condition. Figure 4 shows the curves of the absorption peaks with frequency changes at different dielectric layer thicknesses, ranging from 0.1 mm to 0.5 mm. As can be seen from Figure 4, the intensity of the absorption peaks gradually increase, and the frequencies
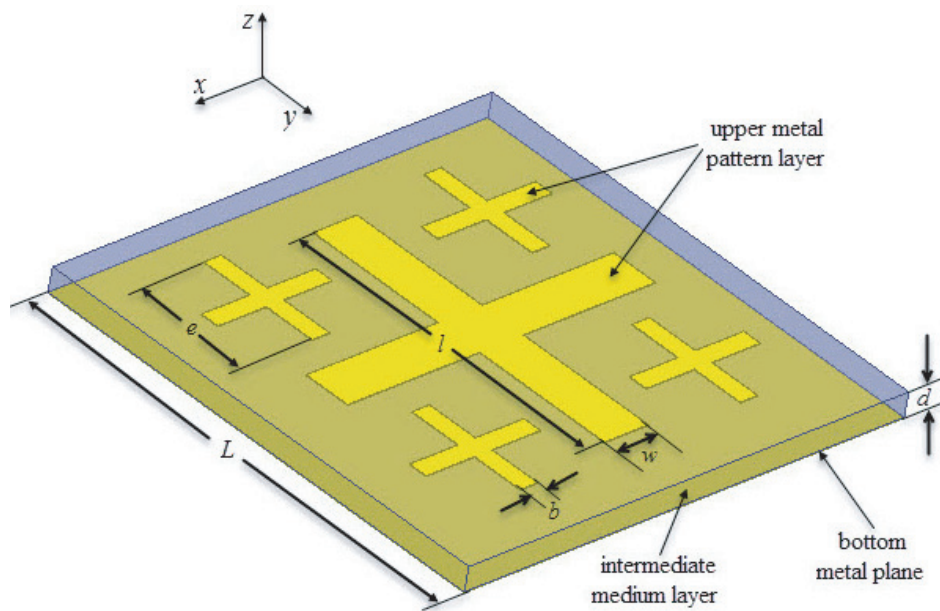

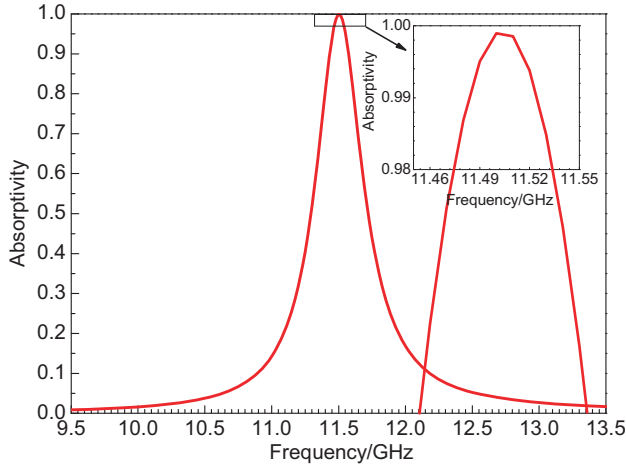**Figure 2.** One unit cell of the cruciform structure absorber.

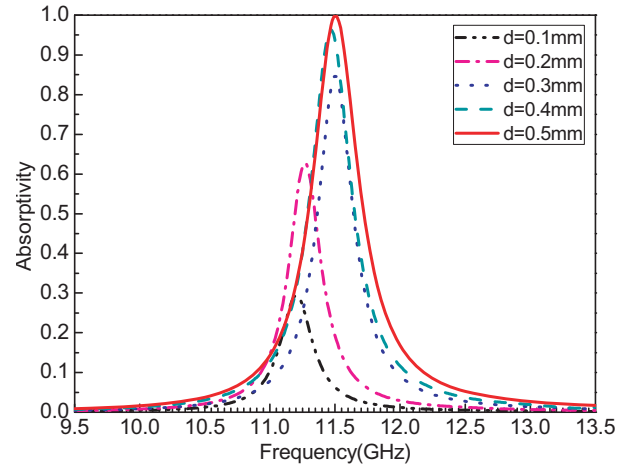**Figure 3.** Simulated absorptivity of the absorber.

Figure 4. Absorptivity of the absorber different the thickness of the medium layer.
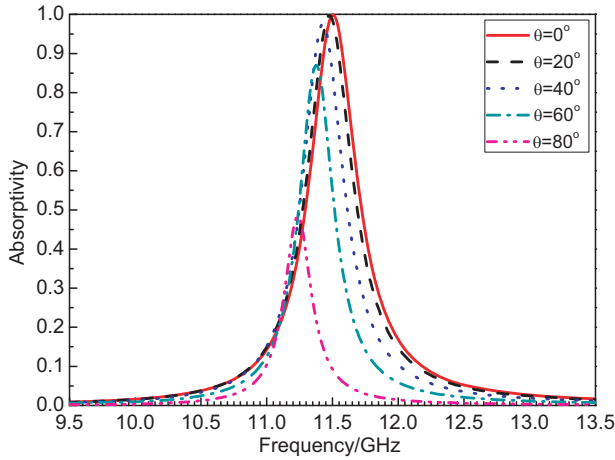

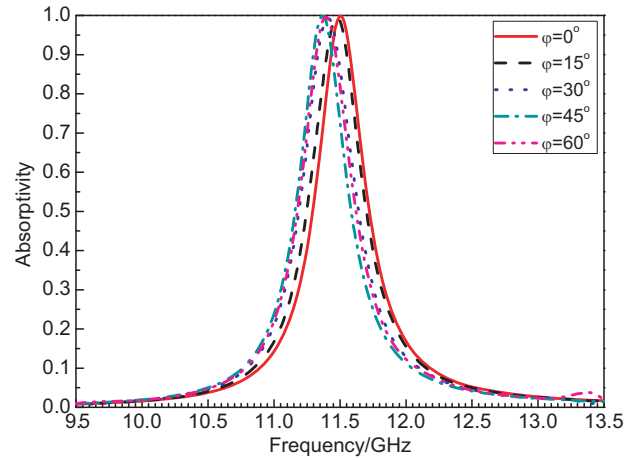**Figure 5.** Absorptivity with different incident angles.

Figure 6. Absorptivity with different polarization angles.

of the absorption peaks are blue-shifted with the increasing thickness of the medium layer. When the thickness equals 0.1 mm, the absorptivity has a value of 29.40% at 11.2 GHz. And yet, when the thickness is increased to 0.5 mm, the absorptivity has a maximum value of 99.99% at 11.5 GHz.

Next, the simulated results that the absorption peaks vary with the incident angle are discussed. Aiming at different incident angles, the respective curves of the absorption peaks varying with incident angle are shown in Figure 5. It is clearly observed that the absorption peaks slightly decrease with increasing incident angles, which range from the normal incidence to 60°. However, when the incident angle is increased to 80°, the absorption peak significantly decreases. In the meantime, from Figure 5, we can see clearly that the frequencies of the absorption peaks are slightly red-shifted with increasing incident angles. As is shown in Figure 5, the absorptivity equals 99.99% at 11.5 GHz, 99.69% at 11.48 GHz, 97.52% at 11.43 GHz, 87.05% at 11.38 GHz and 48.44% at 11.24 GHz when the incident angle equals 0°, 20°, 40°, 60°, 80°, respectively.

Besides, we study how different polarization angles ϕ affect the absorption characteristics under the normal incidence condition. The curves of the absorption peaks with frequency changes at different polarization angles are shown in Figure 6. It is evident from Figure 6 that the trend of the curve distribution shows symmetrical distribution with different polarization angles, which ranges from 30° to 60°, in steps of 15°. This happens because of the symmetrical design of the proposed MMA in

this paper. Meanwhile, the simulated results show that this proposed MMA structure in this paper is isotropic.

The above analysis is based on the numerical simulations. In order to explain the simulated results, the absorption mechanism for the MMA will be given by using reflection theory in the next section.

4. RESULTS AND DISCUSSION

Now we try to use the reflection theory model to explain the physical mechanism of absorption for MMA. Firstly, in order to select correct expressions of the effective EM parameters of the medium layer to analyze the MMA, a graph of the impedance as a function of frequency is shown in Figure 7. It is evident from Figure 7 that the magnitude of impedance is equal to $360.99\,\Omega$ when the absorption frequency equals $11.5\,\text{GHz}$. At this point, we find that the free space wave impedance $377\,\Omega$ is greater than $360.99\,\Omega$ given in Figure 7. According to the relations of Z and Z_0 in Eqs. (1) and (2), Eq. (1) will be applied to analyze the MMA presented in this paper. Eq. (1) shows that not only the dielectric layer thickness, frequency and incident angle but also the loss angle and real part of dielectric permittivity and magnetic permeability have an impact on the absorptivity. Besides, the functional relations between the angle of incidence θ and the angle of refraction α stems from the Snell's law. Here, for convenience, we choose the expression of μ'_1 in Eq. (1) to analyze the MMA presented in this article. Secondly, in order to facilitate the analysis of the relations among absorptivity, incident angles, absorption frequency and dielectric layer thickness, we must set up the functional relation between absorptivity and these variables. Figure 8 shows the retrieved effective permeability from the simulation of the proposed MMA. From Figure 8, we can get the real and imaginary parts of the permeability, which equal 0.7881 and -3.3831 at $11.5\,\text{GHz}$, respectively. Therefore, the loss tangent equals -4.29. Then, the hyperbolic tangent function $\tanh(\frac{\pi}{2}\tan\delta)$ is roughly equal to -1. So, the expression of μ'_1 in Eq. (1) is simplified as

$$\mu'_1 \approx -\frac{\pi c}{2d\omega}\frac{1-\sqrt{1-A(\omega)}}{1+\sqrt{1-A(\omega)}}\frac{1}{\cos\theta} \tag{3}$$

To greatly facilitate the following researches, Eq. (3) is further simplified as

$$\frac{1-\sqrt{1-A(\omega)}}{1+\sqrt{1-A(\omega)}} \approx -\frac{2}{\pi c}\omega\mu'_1 d\cos\theta \tag{4}$$

To get the functional relationships between absorptivity and constitutive parameters, we will try to explore the functional relationships between $[1-\sqrt{1-A(\omega)}]/[1+\sqrt{1-A(\omega)}]$ and $A(\omega)$. $[1-\sqrt{1-A(\omega)}]/[1+\sqrt{1-A(\omega)}]$ as a function of the $A(\omega)$ is plotted in Figure 9. Figure 9 shows

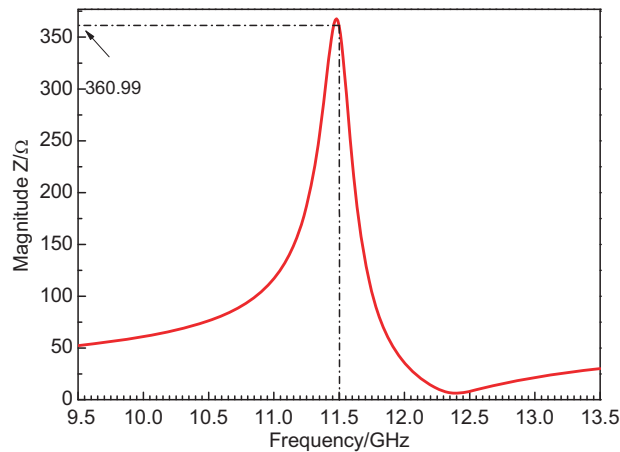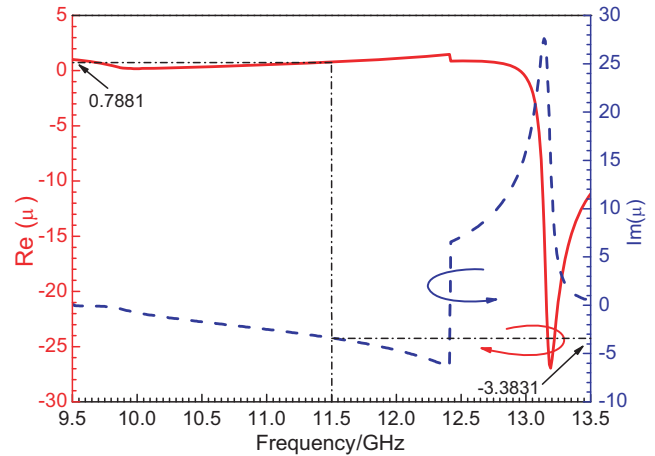**Figure 7.** The magnitude of impedance Z.

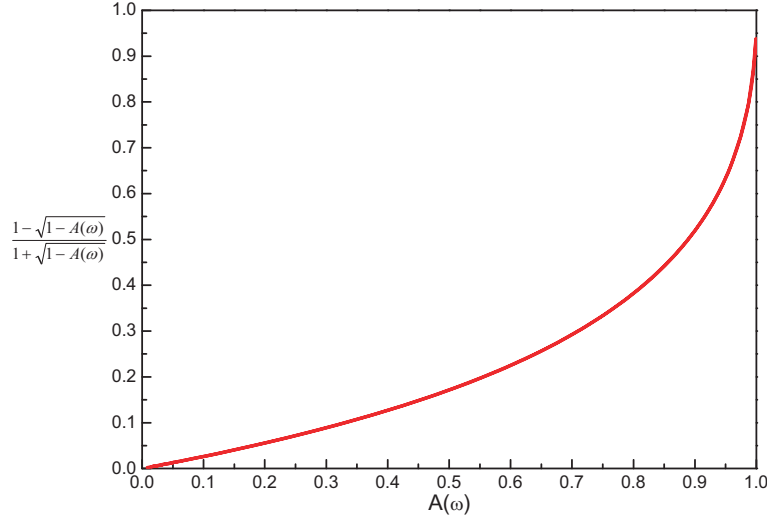**Figure 8.** Retrieved effective permeability.

Figure 9. $[1 - \sqrt{1 - A(\omega)}]/[1 + \sqrt{1 - A(\omega)}]$ as a function of the $A(\omega)$.

that $[1 - \sqrt{1 - A(\omega)}]/[1 + \sqrt{1 - A(\omega)}$ increases by the monotonic increasing function with the increase of the $A(\omega)$. Therefore, Eq. (4) can be approximately expressed as

$$A(\omega) \propto \frac{1 - \sqrt{1 - A(\omega)}}{1 + \sqrt{1 - A(\omega)}} \propto -\omega \mu_1' d \cos \theta \tag{5}$$

Equation (5) indicates that there is a directly proportional relationship between the absorptivity and $-\omega \mu_1' d \cos \theta$. The absorptivity is influenced by the absorption frequency ω, real part of permeability μ_1', dielectric layer thickness d and incident angle θ.

We can see from Figure 4 that as the absorptivity $A(\omega)$, incident angle θ and EM parameters are kept constant, the absorption peaks move to the higher frequency with increasing dielectric layer thickness (blue shift). In order to more clearly show this changing trend, the curves of the absorptivity with the dielectric layer thickness d are drawn in Figure 10. Meanwhile, we find that the changing trend is also shown in Eq. (5). In Eq. (5), the dielectric layer thickness d varies directly as the absorption frequency ω with the absorptivity $A(\omega)$, incident angle θ and EM parameters are kept constant. As shown in Figure 10, however, the relationships between the absorption frequency and dielectric layer thickness are not entirely linear, due to the nonlinear relationship between the frequency ω and the real part of the permeability μ_1' in Eq. (2). Besides, Figure 4 shows that the intensity of the absorption peaks increases with increasing thickness of the medium layer, due to the directly proportional relationship between the absorptivity $A(\omega)$ and the thickness d in Eq. (5). It can be seen from Eq. (5) that the value of absorptivity is inversely proportional to the incidence angle $\theta(0^o \leq \theta \leq 90°)$ when μ_1', d and ω are constant. The absorption peaks varying with the incident angle are presented in Figure 5. As can be seen from Figure 5, the intensity of absorptivity decreases with increasing incidence angle, and the absorption peaks have red shift. Obviously, the varying tendencies of the curves presented in Figure 5 are completely consistent with the inverse relations as indicated in Eq. (5). Furthermore, in order to more clearly show the red-shift phenomenon, the absorption frequency as a function of the incidence angle when the $A(\omega)$ equals 0.4 is shown in Figure 11. From Figure 11, the relationships between the absorption frequency and the incidence angle are not entirely linear, which stems from the effect of the μ_1' and the approximate value of $\tanh(\frac{\pi}{2} \tan \delta)$ in Eq. (2). Here, to emphasize an important point, the relations between the absorptivity and polarization angle ϕ cannot be explained by Eq. (5).

Further, the physical mechanism of the above phenomenon is determined based on the following formula [32].

$$d = (2l + 1) \frac{\lambda_{1eff}}{4} \quad l = -1, -2, -3 \ldots \tag{6}$$

where $\lambda_{1eff} = 2\pi/k_{1eff} = \lambda_1/\cos \alpha$, λ_1 is the wavelength of the EM wave in the medium layer.
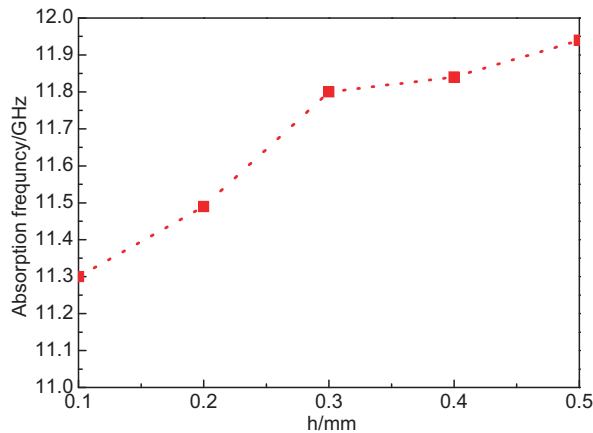
Figure 10. The absorption frequency as a function of the dielectric layer thickness.
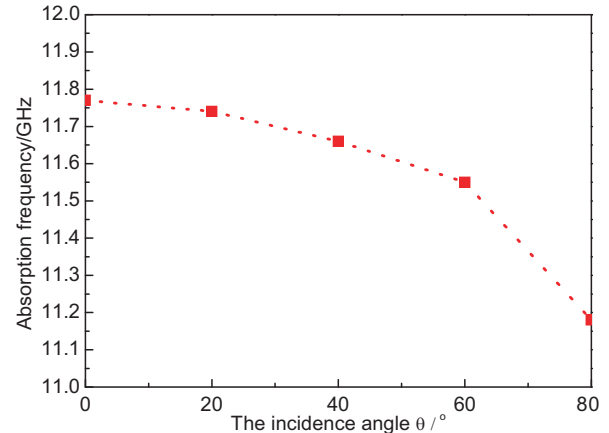

Figure 11. The absorption frequency as a function of the incidence angle.

Equation (6) reveals the relationship between the incident wavelength and thickness of the medium layer. The stable standing waves are formed in the medium layer if the relationship between the wavelength of an incident ray and the thickness of the medium layer satisfies Eq. (6). At this point, the energy of the EM waves residing within the medium layer is absorbed and converted into heat after multiple reflections of the EM waves. It is the nature of the properties of a metamaterial absorber. Therefore, the absorptivity depends on the distance that the EM waves have traveled through the medium layer for certain incident wavelength: the longer the distance is, the greater the absorptivity is. This can explain why the intensity of the absorption peaks increases with increasing thickness of the medium layer in Figure 4, and the intensity of the absorption peaks decreases with increasing angle of incidence in Figure 5. Generally, the intensity of the absorption peaks increases with the thickness of the medium layer. When the thickness of the medium layer increases to the thickness corresponding to one fourth of a wavelength of the incident waves, the absorptivity $A(\omega)$ reaches the maximum. However, the intensity of the absorption peaks decreases with the increase of the incident angles, due to the increasing distance that the incident waves travel when the angle of incidence increases.

5. CONCLUSIONS

In a word, we have analyzed the proposed MMA by using the reflection theory and elaborated on the physics mechanism for the MMA. The influences of the dielectric layer thickness and incident angle on the absorption properties of the MMA are quantificationally investigated. The intensity of the absorption peaks gradually increases, and the frequencies of the absorption peaks are blue-shifted with increasing thickness of the medium layer. Moreover, the intensity of absorptivity decreases with increasing incidence angle, and the absorption peaks have red shift. Based on the reflection theory, several important conclusions from the numerical simulations on the MMA are explained in detail. The numerical simulation results of the MMA are in good agreement with the reflection theory analysis, which further proves the validity of reflection theory model. At the same time, by using the reflection theory model, the relationships between the constitutive parameters and the absorption properties can be more easily understood, which will provide consultation to engineers in design and fabrication of the advanced MMA.

ACKNOWLEDGMENT

REFERENCES

1. Shelby, R. A., D. R. Smith, and S. Schultz, "Experimental verification of a negative index of refraction," *Science*, Vol. 292, 77–79, 2001.
2. Parazzoli, C. G., R. B. Greegor, K. Li, B. E. C. Koltenbah, and M. Tanielian, "Experimental verification and simulation of negative index of refraction using Snell's law," *Phys. Rev. Lett.*, Vol. 90, 2003.
3. Pendry, J. B., "Negative refraction makes a perfect lens," *Phys. Rev. Lett.*, Vol. 85, 2000.
4. Schurig, D. J. J. Mock, B. J. Justice, S. A. Cummer, J. B. Pendry, A. F. Starr, and D. R. Smith, "Metamaterial electromagnetic cloak at microwave frequencies," *Science*, Vol. 314, 977–980, 2006.
5. Landy, N. I., S. Sajuyigbe, J. J. Mock, D. R. Smith, and W. J. Padilla, "Perfect metamaterial absorber," *Phys. Rev. Lett.*, Vol. 100, 207402, 2008.
6. Enoch, S., G. Tayeb, P. Sabouroux, N. Guerin, and P. Vincent, "A metamaterial for directive emission," *Phys. Rev. Lett.*, Vol. 89, 2002.
7. Leonhardt, U. and T. Tyc, "Broadband invisibility by non-euclidean cloaking," *Science*, Vol. 323, 10–112, 2009.
8. Niesler, F. B. P., J. K. Gansel, S. Fischbach, and Wegener, "Metamaterial metal-based bolometers," *Appl. Phys. Lett.*, Vol. 100, 2012.
9. Watts, C. M., X. Liu, and W. J. Padilla, "Metamaterial electromagnetic wave absorbers," *Adv. Mater.*, Vol. 24, 98–120, 2012.
10. Marques, R., J. Martel, F. Mesa, and F. Medina, "Left-handed-media simulation and transmission of EM waves in subwavelength split-ring-resonator-loaded metallic waveguides," *Phys. Rev. Lett.*, Vol. 89, 2002.
11. Wen, Q. Y., H. W. Zhang, Y. S. Xie, Q. H. Yang, and Y. L. Liu, "Dual band terahertz metamaterial absorber: Design, fabrication, and characterization," *Appl. Phys. Lett.*, Vol. 95, 2009.
12. Shen, X. P., T. J. Cui, J. M. Zhao, H. F. Ma, W. X. Jiang, and H. Li, "Polarization-independent wide-angle triple-band metamaterial absorber," *Opt. Express*, Vol. 19, 2011.
13. Li, L., Y. Yang, and C. H. Liang, "A wide-angle polarization-insensitive ultra-thin metamaterial absorber with three resonant modes," *J. Appl. Phys.*, Vol. 110, 2011.
14. Shen, X. P., Y. Yang, Y. Z. Zang, J. Q. Gu, J. G. Han, W. L. Zhang, and T. J. Cui, "Triple-band terahertz metamaterial absorber: Design, experiment, and physical interpretation," *Appl. Phys. Lett.*, Vol. 101, No. 15, 2012.
15. Sun, L. K., H. F. Cheng, Y. J. Zhou, and J. Wang, "Improvement on the wave absorbing property of a lossy frequency selective surface absorber using a magnetic substrate," *Chin. Phys. B*, Vol. 21, 2012.
16. Zhang, H. B., L. W. Deng, P. H. Zhou, L. Zhang, D. M. Cheng, H. Y. Chen, D. F. Liang, and L. J. Deng, "Low frequency needlepoint-shape metamaterial absorber based on magnetic medium," *J. Appl. Phys.*, Vol. 113, 2013.
17. Xu, Y. Q., P. H. Zhou, H. B. Zhang, L. Chen, and L. J. Deng, "A wide-angle planar metamaterial absorber based on split ring resonator coupling," *J. Appl. Phys.*, Vol. 110, 2011.
18. Kim, J., R. Soref, and W. R. Buchwald, "Multi-peak electromagnetically induced transparency (EIT)-like transmission from bull's-eye-shaped metamaterial," *Opt. Express*, Vol. 18, 17997–18002, 2010.
19. Liu, N., M. Mesch, T. Weiss, M. Hentschel, and H. Giessen, "Infrared perfect absorber and its application as plasmonic sensor," *Nano Lett.*, Vol. 10, 2342–2348, 2010.
20. Jiang, Z. H., S. Yun, F. Toor, D. H. Werner, and T. S. Mayer, "Conformal dual-band near-perfectly absorbing mid-infrared metamaterial coating," *ACS Nano*, Vol. 5, 4641–4647, 2011.
21. Wang, J., Y. T. Chen, J. M. Hao, M. Yan, and M. Qiu, "Shape-dependent absorption characteristics of three-layered metamaterial absorbers at near-infrared," *J. Appl. Phys.*, Vol. 109, 2011.
22. Dai, L. and C. Jiang, "Anomalous near-perfect extraordinary optical absorption on subwavelength thin metal film grating," *Opt. Express*, Vol. 17, 20502–20504, 2009.

23. Aydin, K., V. E. Ferry, R. M. Briggs, and H. A. Atwater, "Broadband polarization-independent resonant light absorption using ultrathin plasmonic super absorbers," *Nat. Commun.*, Vol. 2, 2011.

24. Lin, C. H., R. L. Chern, and H. Y. Lin, "Polarization-independent broad-band nearly perfect absorbers in the visible regime," *Opt. Express*, Vol. 19, 415–424, 2011.

25. Han, Y., W. Q. Che, C. Christopoulos, and Y. M. Chang, "Investigation of thin and broadband capacitive surface-based absorber by the impedance analysis method," *IEEE Transactions on Electromagnetic Compatibility*, Vol. 57, 22–26, 2015.

26. Bhattacharyya, S., S. Ghosh, and K. V. Srivastava, "Equivalent circuit model of an ultra-thin polarization-independent triple band metamaterial absorber," *AIP Adv.*, Vol. 4, 2014.

27. Xu, X. H., G. M. Wang, M. Q. Qi, J. G. Liang, J. Q. Gong, and Z. M. Xu, "Triple-band polarization-insensitive wide-angle ultra-miniature metamaterial transmission line absorber," *Phys. Rev. B*, Vol. 86, 2012.

28. Chen, H. T., "Interference theory of metamaterial perfect absorbers," *Opt. Express*, Vol. 20, 7165–7172, 2012.

29. Kong, H., G. Li, Z. Jin, G. Ma, Z. Zhang, and C. Zhang, "Polarization-independent metamaterial absorber for terahertz frequency," *Int. J. Infrared Milli. Waves*, Vol. 33, 649–656, 2012.

30. Grant, J., Y. Ma, S. Saha, A. Khalid, and D. R. S. Cumming, "Polarization insensitive, broadband terahertz metamaterial absorber," *Opt. Lett.*, Vol. 36, 3476–3478, 2011.

31. Huang, L., D. R. Chowdhury, S. Ramani, M. T. Reiten, S. N. Luo, A. K. Azad, A. J. Taylor, and H. T. Chen, "Impact of resonator geometry and its coupling with ground plane on ultrathin metamaterial perfect absorbers," *Appl. Phys. Lett.*, vol. 101, 101–102, 2012.

32. Zhang, Z. H., Z. P. Wang, and L. H. Wang, "Design principle of single- or double-layer wave-absorbers containing left-handed materials," *Mater. Des.*, Vol. 30, 3908–3912, 2009.